The Structure of Tap42/α4 Reveals a Tetratricopeptide Repeat-like Fold and Provides Insights into PP2A Regulation[†,‡]

Jing Yang,[§] S. Mark Roe,[§] Todd D. Prickett,[||] David L. Brautigan,[||] and David Barford*[,§]

Section of Structural Biology, Chester Beatty Laboratories, Institute of Cancer Research, 237 Fulham Road, London SW3 6JB, U.K., and Center for Cell Signaling and Department of Microbiology, University of Virginia School of Medicine, Charlottesville, Virginia 22908

Received April 16, 2007; Revised Manuscript Received May 29, 2007

ABSTRACT: Physiological functions of protein phosphatase 2A (PP2A) are determined via the association of its catalytic subunit (PP2Ac) with diverse regulatory subunits. The predominant form of PP2Ac assembles into a heterotrimer comprising the scaffolding PR65/A subunit together with a variable regulatory B subunit. A distinct population of PP2Ac associates with the Tap42/α4 subunit, an interaction mutually exclusive with that of PR65/A. Tap42/α4 is also an interacting subunit of the PP2Ac-related phosphatases, PP4 and PP6. Tap42/α4, an essential protein in yeast and suppressor of apoptosis in mammals, contributes to critical cellular functions including the Tor signaling pathway. Here, we describe the crystal structure of the PP2Ac-interaction domain of *Saccharomyces cerevisiae* Tap42. The structure reveals an all α-helical protein with striking similarity to 14-3-3 and tetratricopeptide repeat (TPR) proteins. Mutational analyses of structurally conserved regions of Tap42/α4 identified a positively charged region critical for its interactions with PP2Ac. We propose a scaffolding function for Tap42/α4 whereby the interaction of PP2Ac at its N-terminus promotes the dephosphorylation of substrates recruited to the C-terminal region of the molecule.

The serine/threonine-specific protein phosphatase 2A (PP2A)[1] functions to control signal transduction pathways that regulate cell proliferation, growth, apoptosis, and progression through the cell cycle (*1*, *2*). Distinct functions of PP2A, mediated by the diversity of its holoenzyme structure, are generated on association of its catalytic subunit with a variety of scaffolding and regulatory subunits. The latter specify phosphatase activity toward defined substrates and determine its intracellular localization (*3*−*7*). Most PP2A corresponds to a constant AC heterodimer of the catalytic (PP2Ac) and scaffolding (PR65/A) subunits, able to associate with a variety of regulatory B subunits. A much smaller proportion of PP2Ac (5−10%), not in complex with the PR65/A subunit, is instead associated with a structurally distinct protein, Tap42, first identified in yeast as a type *t*wo *A* phosphatase interacting *p*rotein (42 kDa), due to its capacity to suppress *sit4* mutations (*8*). Alpha4, the mammalian homologue of Tap42, binds directly to PP2Ac, at the exclusion of the A and B subunits, suggesting overlapping sites on PP2Ac for Tap42 and PR65/A (*9*, *10*). This is consistent with genetic studies in yeast showing that inactivation of Tpd3 and Cdc55 (*Saccharomyces cerevisiae* A and B subunits) enhances Tap42 association with Pph21/Pph22 (*11*) and implies a balance between the population of PP2Ac in complex with Tap42 and PR65/A. In contrast to PR65/A that binds only to PP2Ac (α and *β* isoforms in mammals, Pph21 and Pph22 in yeast), Tap42 is also an interacting subunit of the PP2Ac-like phosphatases PP4 and PP6 (Sit4 and Pph3 in yeast) (*8*, *12*).

Tap42 is essential for yeast viability (*8*), possibly owing to its participation in the rapamycin-sensitive Tor signaling pathway. In yeast, the association of Tap42 with type 2A phosphatases is disrupted by both rapamycin and nutrient deprivation, conditions that suppress Tor activity (*8*, *11*). Interestingly, at the permissive temperature, ts *tap42* mutants confer weak resistance to rapamycin (*8*, *13*). However, the molecular mechanisms of these semidominant mutants, which are defective in their interactions with Pph21/Pph22 (*13*, *14*), are not well understood.

Other roles of Tap42/α4 have recently been identified. In murine cells, α4 functions as an essential inhibitor of apoptosis via its ability to promote dephosphorylation of the transcription factors p53 and c-Jun (*15*). Deletion of α4 results in expression of proapoptotic genes with concomitant cell death. Tap42−PP2Ac complexes are also required for the cell-cycle-dependent distribution of actin, via a Rho-GTPase-dependent mechanism (*16*). Tap42/α4 is capable of modulating the substrate specificity of PP2Ac (*9*) and exerts opposing allosteric effects on PP2Ac and PP6 (*17*). Although only a few potential substrates of Tap42−α4-phosphatase complexes have been defined, Tap42-mediated modulation of phosphatase activity explains how rapamycin-induced disassembly of Tap42−phosphatase complexes may induce the dephosphorylation of some substrates, while enhancing the phosphorylation of others (*13*, *18*).

[†] The work in D.B.'s laboratory was funded by CR-UK, and that in D.L.B.'s laboratory was supported by U.S. Public Health Service Grant CA-77584 from the NCI, National Institutes of Health.

[‡] Coordinates and structure factors have been deposited with the Protein Data Bank (ID codes 2v0p and r2v0psf, respectively).

* Corresponding author. E-mail: david.barford@icr.ac.uk. Tel: 020 7153 5420. Fax: 020 7153 5457.

[§] Institute of Cancer Research.

[||] University of Virginia School of Medicine.

[1] Abbreviations: PP2A, protein phosphatase 2A; PP2Ac, protein phosphatase 2A catalytic subunit; PP4, protein phosphatase 4; PP6, protein phosphatase 6; Tap42, two A phosphatase interacting protein (42 kDa); Tor, target of rapamycin; TPR, tetratricopeptide repeat.

10.1021/bi7007118 CCC: $37.00
Published on Web 07/06/2007

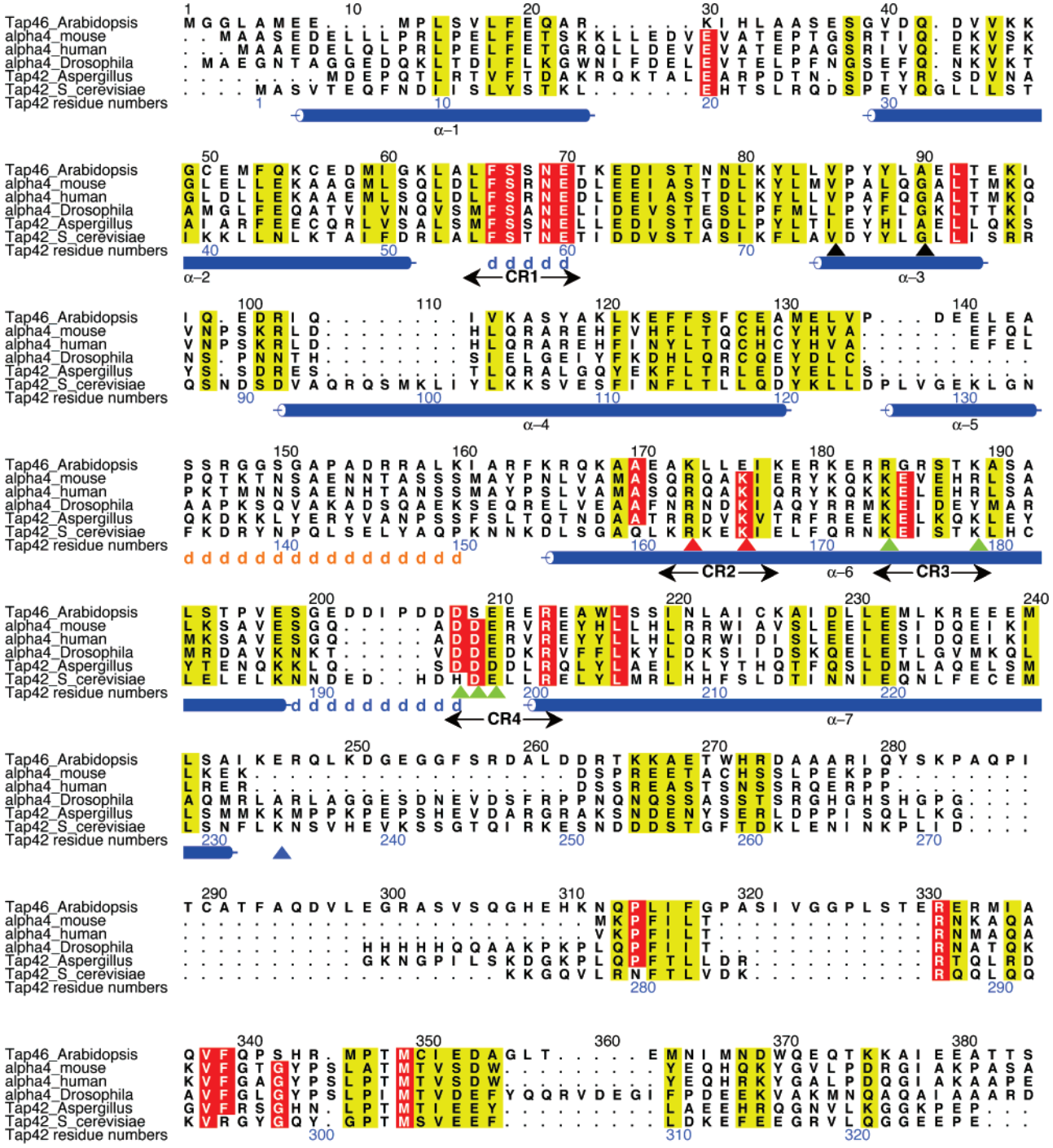

FIGURE 1: Multiple sequence alignment of Tap42/α4 showing the position of conserved (yellow) and invariant (red) residues, location of α-helices, and residues mutated in this study. Mutation of residues denoted by red arrows abolishes Tap42−PP2Ac interactions, whereas mutation of residues indicated by green arrows does not affect PP2Ac interactions. The blue arrow indicates the C-terminus of the crystallized Tap42ΔC, and black arrows indicated ts mutations (*tap42-11*). d = disordered regions (MolA, blue; MolB, amber). Structurally conserved regions (CR1−CR4) are indicated. This figure was prepared using ALSCRIPT (*42*).

Yeast Tap42 is a protein of 366 residues that shares no sequence similarity to any other protein (including PR65/A) and is therefore expected to adopt a novel fold. Domain mapping of murine α4 demonstrates that only the N-terminal 249 residues are required for PP2Ac interactions, with the central 100 residues alone being capable of mediating weak interactions (*19*, *20*). The C-terminal region defines interactions to a PP2A substrate, the Opitz syndrome phosphoprotein Mid1 (*20*). To visualize the structure of Tap42 and to understand how it interacts with PP2Ac, we have determined the structure of its PP2Ac-binding domain. The structural data reveal an all-α-helical fold, reminiscent of tetratricopeptide repeat and 14-3-3 proteins. A mutagenesis screen indicates that the PP2Ac-binding site involves a positively charged conserved region of the protein.

EXPERIMENTAL PROCEDURES

Expression and Purification of S. cerevisiae Tap42. Yeast Tap42 was amplified by PCR and cloned into *Nde*I and *Xho*I sites of the pTWO-B vector. Generation of the recombinant baculovirus using the GIBCO/Life Sciences Bacmid system was performed using standard procedures. *Sf*9 cells were

Table 1: Crystallographic Data Collection and Refinement Statistics

parameter	
space group, *N*	*P*1, 2
a (Å)	44.9
b (Å)	48.4
c (Å)	71.9
α (deg)	81.4
β (deg)	87.9
γ (deg)	69.6
X-ray source	ESRF, BM14
wavelength (Å)	0.9775
resolution range (Å)	30−1.8 (1.9−1.8)
observations (*N*)	219673
completeness[a] (%)	96.4 (96.4)
multiplicity[a]	4.4 (4.4)
R_{merge}[a]	0.047 (0.456)
I/σ_I[a]	15.6 (2.6)
protein atoms (*N*)	3562
ligand atoms (*N*)	4 (Zn)
solvent atoms (*N*)	253
R_{cryst}[a]	0.217 (0.315)
R_{free}[a]	0.281 (0.371)
mean *B*	32
rmsd bond lengths (Å)	0.020
rmsd bond angles (deg)	1.814
allowed, additionally allowed (%)	95.4, 4.6

[a] Highest shell in parentheses. Disordered regions: MolA, Phe56−Glu60 and His196−Arg207; MolB, Asn134−Pro149.

lysed 48 h postinfection. The protein was purified by Ni-NTA (Qiagen), the His_6 tag was cleaved overnight, and the protein was further purified using Mono Q and S75 gel filtration chromatography (Amersham) and concentrated to 10 mg/mL before crystallization screening.

Expression and Purification of Tap42ΔC. Tap42 (residues 1−234) was amplified by PCR and cloned into *Bam*HI and *Not*I sites of the pGEX-6P-1 vector. Expression of this protein was performed at 20 °C overnight in *Escherichia coli* strain B834. Tap42ΔC was purified by glutathione−Sepharose affinity (Amersham), GST cleavage, S75 gel filtration, and MonoQ ion exchange (Amersham). Selenomethionine-labeled protein was grown in minimal media and purified as for the native protein.

Crystallization of Tap42ΔC. The protein was concentrated to 10 mg/mL before crystallization. Crystals were grown at 20 °C using the hanging drop method. One microliter of protein was mixed with an equal volume of crystallization buffer: 20% (w/v) PEG 8000, 0.1 M sodium cacodylate, pH 6.5, 0.2 M magnesium acetate, and 2 mM DTT. Crystals, belonging to space group *P*1, were optimized by seeding.

Structure Determination. The structure was determined using a single SeMet-labeled crystal using data collected to 1.8 Å at BM14, ESRF, Grenoble, France. Data were processed using MOSFLM and SCALA (*21*). The structure was determined using SHELXC/D/E, with polypeptide chain tracing performed by ARP/WARP (*22*), and the structure was refined using REFMAC (*21*). Model building was performed using COOT (*23*).

Mutagenesis, Cell Culture, and Immunoprecipitation. Murine α4 cloned in the pcDNA3-FLAG vector was mutated with the following PCR primers: R156E/K159D forward 5′-GGCATCTCAAGAACAGGCTGACATAGAGAG-3′, R156E/K159D reverse 5′-GTATCTCTCTATGTCAGCCTGTTCTTGAGATG-3′, K167E/R172E forward 5′-GCAGAGGGAGGAGGTGGAGCATAGGTTGTCTG-3′, K167E/R172E reverse 5′-GCAGACAACTCATGCTCCACCTCCTCCTTCTG-3′, D186A/D187A/E188A forward 5′-GGTCAAGCACGTCGTAAAGCGGTTCGGG-3′, and D86A/D187A/E188A reverse 5′-CCCGAACGCGTTTACGACGTGCTTGACC-3′. HEK293T cells were grown in modified Eagle's medium supplemented with 10% fetal bovine serum and 2 mM L-glutamine at 37 °C in a humidified incubator with 5% CO_2. Cells were transfected with 5 μg of FLAG-α4 constructs using Arrest-In (Open Biosystems) as described in the manufacturer's protocol and incubated for 24 h prior to harvesting. Cells were lysed in a 1% NP-40 buffer [1% NP-40 (IGE-PAL 640), 50 mM MOPS, pH ∼7.5, 150 mM NaCl, 1 mM Pefabloc (Sigma), 1 μg/mL pepstatin, 1 μg/mL leupeptin, 1 μM microcystin-LR (Alexis Biochemical), 1 mM sodium fluoride, 1 mM sodium orthovanadate, and 1 mM dithiothreitol]. Extracts were recovered as supernatants after centrifugation at 13200 rpm for 15 min at 4 °C. Approximately 750 μg of soluble protein was immunoprecipitated using anti-FLAG beads (M2-Sigma) for 2 h at 4 °C with gentle mixing and washed two to three times with NP-40 buffer. Anti-FLAG M2 beads were taken up in 40 μL of 2× SDS Laemmli buffer, boiled for 5 min at 100 °C, and analyzed by immunoblotting with anti-Mid1 (Dr. Timothy Cox, University of Washington; 1:1000), anti-PP2Ac (peptide antibody; 1:5000), anti-PP6 (peptide antibody; 1:5000), and anti-FLAG (Sigma-Aldrich; 1:4000) antibodies.

RESULTS

Structure Determination. We expressed *S. cerevisiae* TAP42 and human α4 using the baculovirus/insect cell system and purified the recombinant proteins using a combination of Ni-NTA, Mono Q ion-exchange, and gel filtration chromatography. Human α4 failed to crystallize; however, extensive crystallization screening of the purified Tap42 protein yielded a single condition where small, relatively poorly formed crystals appeared within 3 months. Determination of the relative molecular mass of protein recovered from the crystallization drop indicated limited proteolysis and truncation of the full-length protein (42 kDa) into two species of approximately 26 and 27 kDa (data not shown). This finding suggested that the truncated protein, rather than full-length Tap42, was responsible for the small crystals. Elective limited trypsinolysis of full-length Tap42 and human α4 yielded similar protease-resistant products of ∼26 kDa, similar in size to the truncated form of Tap42 obtained by spontaneous degradation. Edman sequencing revealed an intact N-terminus indicating a protease-resistant N-terminal region. We estimated a likely C-terminal cleavage site by use of bioinformatics data. Multiple sequence alignments of Tap42 homologues from yeast to human indicate two distinct conserved segments, separated by a region of ∼40 amino acids of low sequence conservation corresponding to the site of sequence insertions present in yeast Tap42 and plant Tap46 relative to mammalian α4 [residues 233−250 of *S. cerevisiae* Tap42 (Figure 1)]. Moreover, protein disorder [RONN (*24*)] and secondary structure prediction [PHYRE (*25*)] programs suggested that the C-terminal ∼130 residues are likely to comprise little to no ordered structure. On the basis of this analysis and the size of the trypsinolysis product, we predicted Lys234 of *S. cerevisiae* Tap42 as the C-terminal trypsin cleavage site (Figure 1). Recently, Smetana et al. (*26*) reported protease-

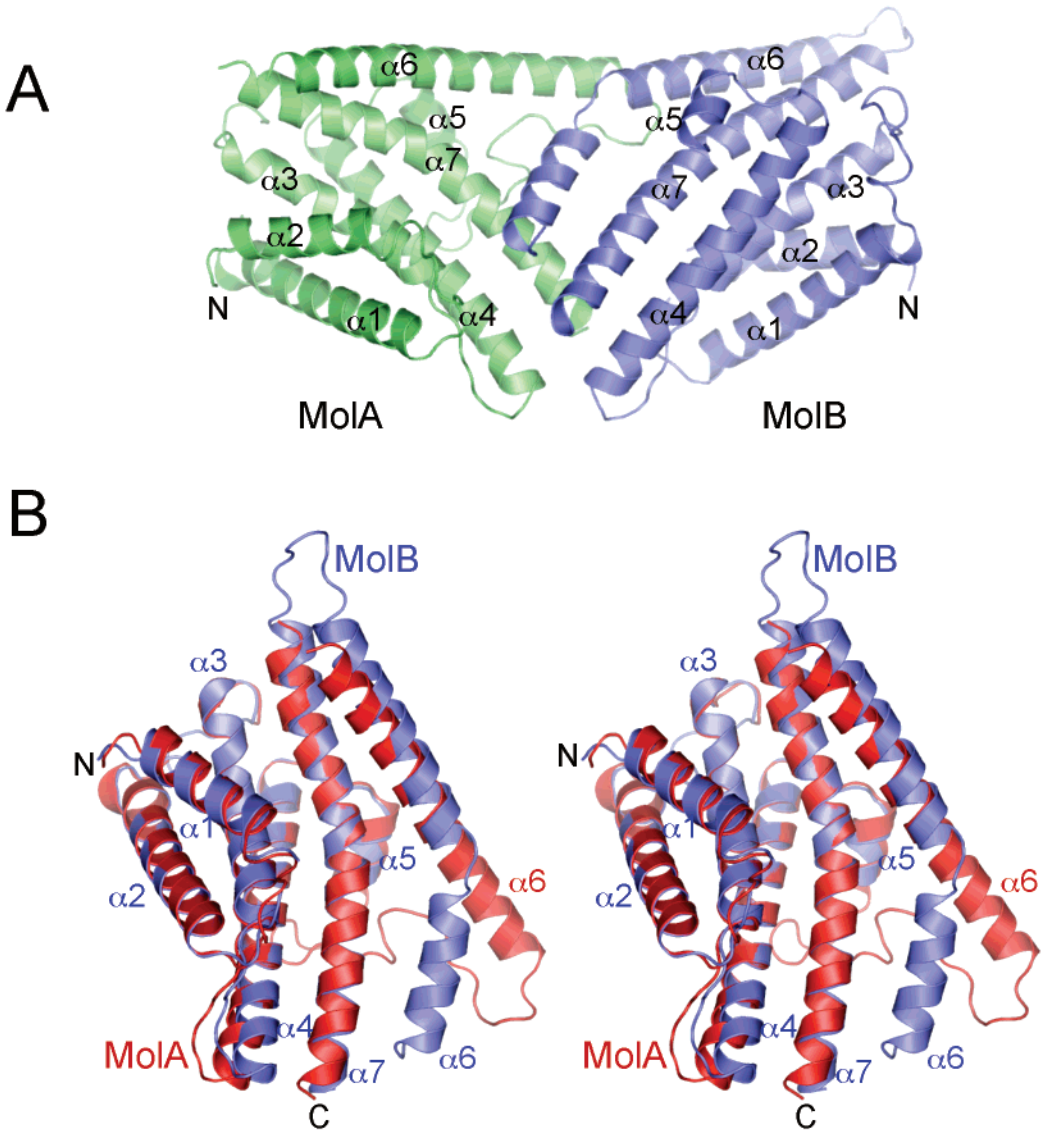

FIGURE 2: (A) View of the Tap42ΔC asymmetric homodimer as viewed in the *P*1 unit cell. The N-termini of α6 participate at the dimer interface, forming different interactions with the opposite molecule of the dimer. MolA and MolB of Tap42ΔC adopt distinct conformations. (B) Stereoview of a superimposition of the two molecules showing how the N-terminus of α6 is kinked by 40° in MolB relative to MolA. The figures were prepared using PYMOL (http://www.pymol.org).

sensitive sites within the region spanning residues 220−254 of human α4 (and equivalent regions of Tap42), in agreement with our findings. Circular dichroism spectra, demonstrating a higher helical content for the N-terminal 222 residues of human α4, relative to the full-length protein, are also supportive of the notion that the region C-terminal to sites of proteolysis of Tap42/α4 adopts little ordered secondary structure (*26*).

The cDNA encoding Met1−Lys234 of *TAP42* (termed Tap42ΔC) was cloned into pGEX-6P-1 and expressed in *E. coli* as a GST fusion protein. Subsequent to glutathione−agarose purification, Tap42ΔC cleaved from GST was purified as for the full-length protein. The protein at 10 mg/mL was crystallized at pH 6.5 and 20 °C by the hanging drop vapor diffusion procedure. SAD X-ray diffraction data to 1.8 Å resolution were collected at ESRF (BM14) from a selenomethionine-labeled crystal (Table 1). The two molecules (termed MolA and MolB) of Tap42ΔC in the *P*1 unit cell were refined independently. Molecules A and B are well-defined in the electron density maps, although two loops in MolA and one in MolB are disordered (Figure 1, Table 1).

Tap42 Adopts a TPR-like Fold. In the *P*1 unit cell, two molecules of Tap42ΔC adopt an asymmetric homodimer (Figure 2A). Formation of this dimer is likely to have been promoted on crystallization, since size exclusion chromatography (data not shown) and small-angle X-ray scattering (*26*) are consistent with a monomeric species in solution. Least-squares superimposition of the two noncrystallographically related molecules reveals essentially similar structures, except for notable differences in the conformation of the α6 helix, responsible for the asymmetric homodimer (discussed below). This results in an overall rmsd of 3.4 Å for 199 superimposed Cα atoms, although a highly conserved core of 124 Cα atoms superimposes within 0.5 Å (Figure 2B).

Tap42ΔC adopts an all-α-helical conformation with a total of seven helices organized in an antiparallel arrangement, with overall dimensions of 65 Å by 35 Å by 25 Å (Figure 3). These dimensions are close to the 72 Å estimated for a truncated version of human (α4Δ222, equivalent to Tap42ΔC) determined using small-angle X-ray scattering (*26*). Tap42/α4 differs in structure from the other PP2Ac-interacting

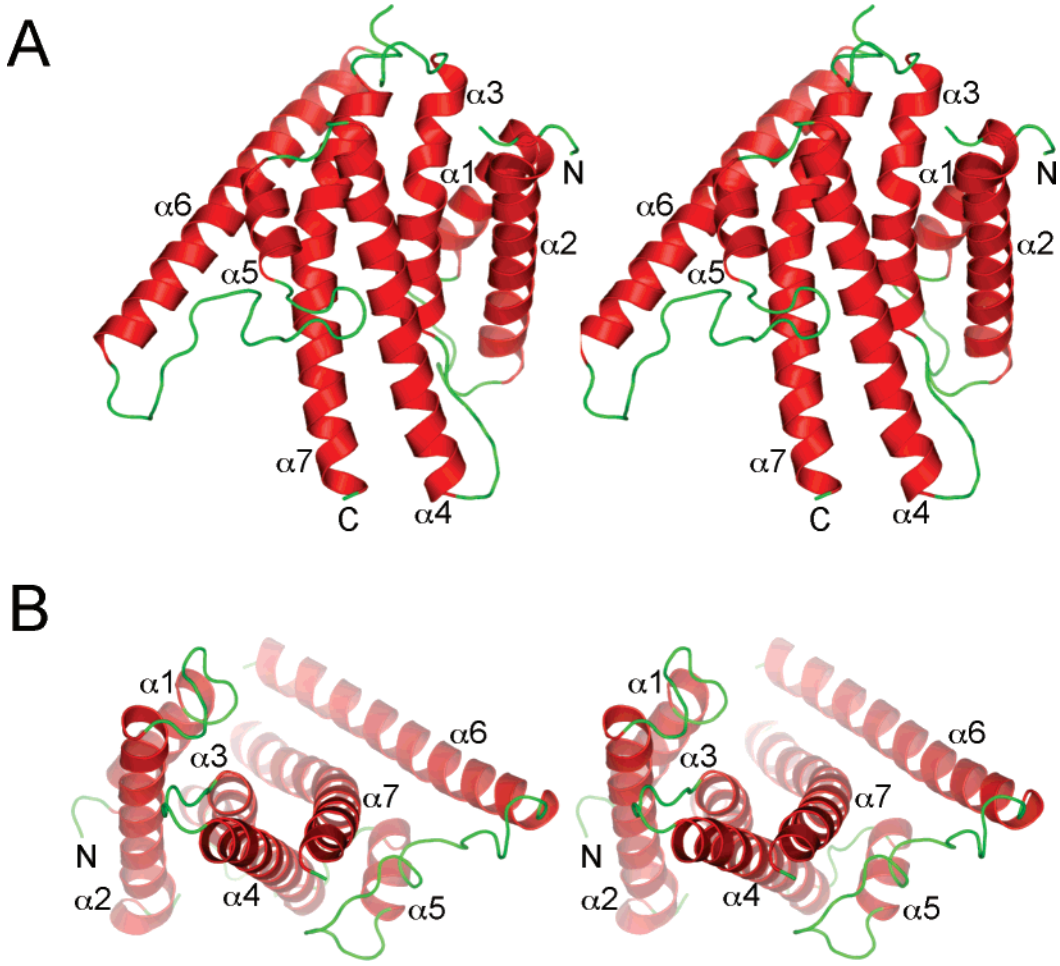

FIGURE 3: Orthogonal views of Tap42ΔC (MolA) illustrating how the seven α-helices of the molecule create opposing concave and convex surfaces. The convex surface is shown in (A).

Table 2: Closest Structural Relatives of Tap42ΔC As Defined by DALI

protein	PDB ID	*Z*-score	rmsd (Å)	no. of aligned residues	% sequence ID	ref
Sec17	1qqe	7.6	3.9	101	7	*29*
SMG7	1ya0	7.1	5.9	118	8	*30*
p67^{phox}	1e96	6.7	2.8	99	12	*31*

protein PR65/A, a multiple HEAT repeat all-α-helical protein (*27*). A search for known protein folds with possible structural similarities to Tap42ΔC using DALI (*28*) revealed the most significant structural similarities to other all-α-helical proteins (Table 2). The three proteins with the highest DALI *Z*-score, a measure of the structural similarity in standard deviations above that expected between two molecules, are the vesicular transport protein Sec17 (*29*), the 14-3-3-like domain of the nonsense-mediated mRNA decay protein SMG7 (*30*), and the TPR motif domain of p67^{phox} (*31*) (Figure 4). Significantly, these proteins perform similar functions as scaffolding and adaptor molecules. Common to all is the antiparallel arrangement of α-helices that creates an extended molecular surface suitable for mediating protein−protein interactions (Figures 3 and 4). In TPR proteins, each TPR motif of 34 amino acids forms a pair of α-helices (termed A and B) oriented in an antiparallel arrangement (*32*). Since adjacent TPR motifs stack in parallel, this creates a regular array of antiparallel α-helices. Strikingly, the uniform right-handed ~25° crossover angle of each helix relative to its neighbor creates a concave molecular surface, lined by the A-helices. In the TPR domains of both HOP and PP5, the concave surface functions as a docking surface for the extended C-terminal five residues of Hsp70/Hsp90 (*33*, *34*), a mode of protein−protein recognition shared with 14-3-3 phosphopeptide complexes (*35*). In a novel arrangement, the TPR intrarepeat turns of p67^{phox} contact Rac in the Rac−p67^{phox} complex (*31*), similar to the interactions between the TPR and phosphatase domains of PP5 (*34*).

Relative to Sec17, SMG7 and p67^{phox}, the α-helices of Tap42ΔC in general, adopt a less regular configuration. In Tap42ΔC, only the N-terminal four helices adopt a regular helical hairpin arrangement, and these superimpose closely with two adjacent TPR motifs of p67^{phox} (TPR2 and TPR3, Figure 4). Additionally, α7 of Tap42ΔC is structurally equivalent to, and aligns with, the A-helix of the fourth TPR motif of p67^{phox}, packing parallel with α3. The intervening helix pair (α5 and α6) is structurally equivalent to the B-helix of TPR4 and a C-terminal α-helix of p67^{phox}, although with inverted orientations (Figure 4). Therefore, although the relative topology of the N-terminal four helices of Tap42ΔC are equivalent to those of two adjacent TPR motifs, the C-terminal three helices of Tap42ΔC are structurally equivalent to, but topologically distinct from, subsequent TPR motifs. Another difference between Tap42ΔC and TPR proteins is that whereas the canonical TPR helices are ~15 residues in length, α-helices of Tap42ΔC tend to be longer, with α4, α6, and α7 twice the length of TPR α-helices, a feature more reminiscent of 14-3-3 proteins (*36*, *37*).

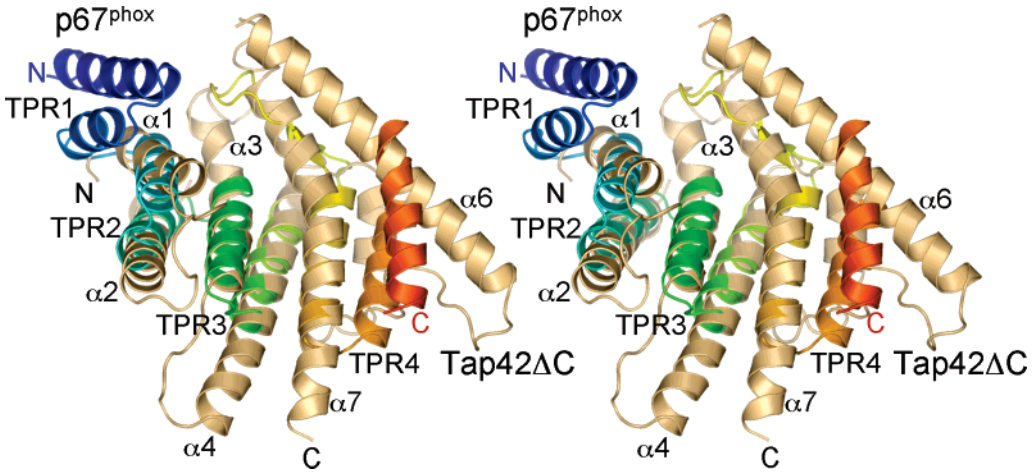

FIGURE 4: TAP42ΔC adopts a TPR/14-3-3-like fold. Stereoview showing a superimposition of MolA onto the TPR domain of p67^{phox} [PDB ID 1e96 (*31*)]. TAP42ΔC is colored in amber, and p67^{phox} is colored from blue to red denoting N- to C-termini. α-Helices 1−4 of TAP42ΔC align closely with the second and third TPR motifs of p67^{phox}, whereas α7 of TAP42ΔC aligns with helix A of the fourth TPR motif.

Similarly to the TPR domain of p67^{phox} and the 14-3-3/TPR-like domains of SMG7 and Sec17, the antiparallel α-helices of Tap42ΔC generate an asymmetric structure featuring a concave surface opposite a more convex surface (Figure 3). In Tap42ΔC, the longer and altered orientation of α6 relative to its counterparts in p67^{phox} and SMG7, results in a less open concave face (Figure 4).

MolA and MolB Are Structurally Nonequivalent, Creating Homodimer Asymmetry. MolA and MolB of Tap42ΔC are structurally nonequivalent. The most pronounced nonequivalence occurs at the N-terminus of α6 and linker region connecting α5 to α6 (Figure 2B). In MolA, the long linker (22 residues) connecting α5 and α6 is well ordered and clearly resolved in the electron density maps. α6 adopts a regular linear α-helix of some 31 residues. In contrast, in MolB, the linker connecting α5 and α6 is disordered, and the N-terminus of α6 is displaced related to its counterpart in MolA. This displacement is caused by a kink at the center of α6 of MolB, dramatically bending the helix at its center by almost 40°. Notably, the altered alignment of the α6 N-terminus in MolB allows it to pack antiparallel with α7, being now structurally similar to the parallel packing of A-helices of adjacent TPR motifs (Figure 2B).

Analysis of homodimer contacts indicates that these are formed mainly from the N-terminus of α6 and C-terminus of α7, with additional contacts provided by the N-terminus of α4 (Figure 2). The differing conformation of α6 in MolA and MolB therefore creates an asymmetric dimer interface. Modeling indicates that, within the context of a dimer, MolA cannot adopt the MolB α6 conformation due to steric overlap with MolB α6, whereas the converse is possible. Examination of crystal lattice contacts indicates that were α6 in MolB to adopt the MolA conformation, a steric clash with a symmetry-related molecule would occur. Asymmetry of the Tap42 homodimer is therefore a function of the crystal-packing environment and, unlike the CHIP asymmetric homodimer (*38*), is most likely not an inherent feature of the protein. We cannot determine which conformation of α6 is the most physiologically relevant, although since crystal packing influences the conformation of α6 in MolB, we predict MolA may represent a more biologically relevant conformation. However, our data reveal that the conformation of α6 is dynamic and capable of adopting two distinct conformations, both of which may be sampled in solution.

Conserved Regions Map to the Interhelix Turns and the Convex Surface. To identify putative functional regions of Tap42ΔC responsible for PP2Ac interactions, we defined the position of highly conserved and invariant residues, derived from a multiple sequence alignment of mammalian α4, Tap42, and Tap46 sequences (Figure 1), on the molecular structure. Conserved residues are mainly confined to the α6 and α7 helices and the interhelix turn connecting α2 and α3, creating four distinct, but closely connected regions of conservation, termed CR1−CR4 (Figure 5). Strikingly, invariant residues of CR2, CR3, and CR4 correspond to solvent-exposed charged amino acids. Residues of CR1 play a role to stabilize the overall structure of the protein; Phe56 is a buried hydrophobic residue, whereas the side chain of Ser57 caps the C-terminus of α1 (Figure 5A). Regions of conservation lie on the same convex surface of the molecule. CR2 is formed from the N-terminus of α6, a region of conformational difference between MolA and MolB. Due to the abundance of Arg and Lys residues, the N-terminus of α6 features a pronounced positive electrostatic potential (Figure 5C).

A temperature-sensitive *TAP42* mutant (*tap42-11*) is defective in PP2Ac interactions (*8*, *14*). The two *tap42-11* mutations (Val75 and Gly80) are conserved buried residues of the α3 helix (Figure 1). Mutation of Val75 to a more bulky isoleucine would disrupt packing contacts between α3 and neighboring α1 and α2 helices, whereas substitution of an acidic glutamate residue for Gly80 would interfere with the hydrophobic core between α3, α4, and α7 (Figure 5A). Mutations at these sites would likely destabilize the entire Tap42ΔC domain with concomitant disruption of PP2Ac interactions.

CR2 Interacts with the PP2A Catalytic Subunit. To examine which of the conserved regions of Tap42ΔC contribute to its interactions with PP2Ac, we tested the binding of FLAG-tagged murine α4 with endogenous PP2Ac by coprecipitation. Murine α4, which shares 22% identity and 45% similarity with *S. cerevisiae* Tap42, was mutated by either charge reversal (Arg to Glu or Lys to Asp) or alanine scanning. Mutations were introduced into CR2, CR3, and CR4. Residues of CR1 were not mutated, since this region of the protein is not required for PP2Ac association (*19*). Cells were transfected with control empty vector and FLAG-tagged wild-type and mutant α4 [α4^{WT}, α4^{CR2} (R163E/

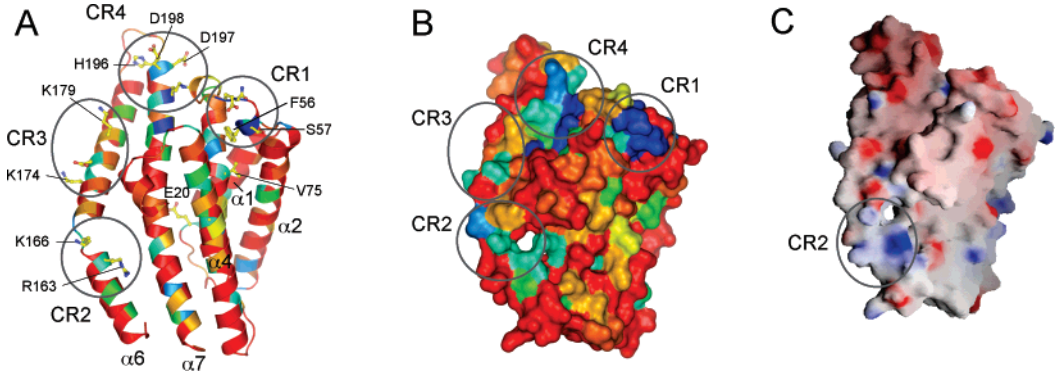

FIGURE 5: Conserved residues of Tap42ΔC form four conserved regions (CR1−CR4). Ribbons (A) and surface (B) views of the position of conserved residues. Color ramping from red to blue denotes weak to high sequence conservation. Those in CR2 at the N-terminus of α6 are required for mediating PP2Ac interactions. (C) CR2 lies in a positive electrostatic potential suitable for interactions with the negatively charged PP2Ac. This figure was produced using GRASP (*43*). MolB is shown, which has an ordered CR1 (Figure 1).

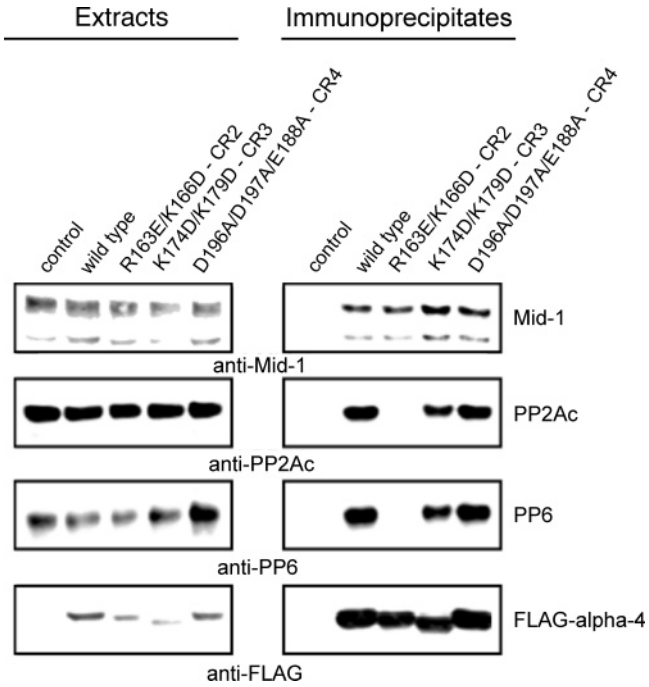

FIGURE 6: Mutational analysis of residues in murine α4 required for association with type 2A protein phosphatases. HEK293T cells were transfected with the empty vector or with one the following FLAG-α4 constructs; wild type, R163E/K166D (CR2), K174E/R179E (CR3), or D196A/D187A/D198A (CR4) (*S. cerevisiae* residue numbering). Immunoprecipitates with anti-FLAG (M2) beads were analyzed by immunoblotting with anti-Mid1, anti-PP2Ac, anti-PP6, and anti-FLAG. The panels show immunoblots of endogenous Mid1 in extracts and precipitates (top) and PP2Ac and PP6 in extracts and immunoprecipitates. The bottom panel shows immunoblots of FLAG-α4 in extracts and anti-FLAG precipitates.

K166D), $\alpha4^{CR3}$ (K174E/R179E), and $\alpha4^{CR4}$ (D196A/D197A/E198A)], and extracts were prepared and immunoprecipitated using anti-FLAG (M2) beads. Murine $\alpha4^{WT}$, $\alpha4^{CR3}$, and $\alpha4^{CR4}$ coprecipitated endogenous Mid1, PP2Ac, and PP6 (Figure 6), indicating that charged residues of CR3 and CR4 were not required for PP2Ac association. In contrast, $\alpha4^{CR2}$ coprecipitated Mid1 but not PP2Ac or PP6. The control lane with empty vector shows no precipitations of any of these proteins. These results suggest that at least either Arg163 and/or Lys166 of the α6 N-terminus (CR2) is/are required for α4 to associate with both PP2Ac and PP6 but not Mid1.

DISCUSSION

A Mechanism for a Tap42ΔC−PP2Ac Complex. Together, our crystallographic and biochemical data provide insights into the structural features of a Tap42−PP2Ac complex. Previous studies had defined the N-terminal 240 residues of murine α4 (equivalent to 270 of *S. cerevisiae* Tap42) as necessary and sufficient for PP2Ac interactions (*19*, *20*). This region of Tap42/α4 corresponds to a protease-resistant, structurally conserved domain: Tap42ΔC (this study and ref *26*). Tap42ΔC is an all-α-helical protein with striking structural similarity to TPR and 14-3-3 proteins, molecules that function as adaptors and scaffolds (*39*). The uniform angular and spatial arrangement of α-helices generates a concave "groove"-like surface opposite a convex face. We investigated likely sites of interaction between Tap42/α4 and PP2Ac by mutating highly conserved residues. Basic residues within CR2 (Arg163 and Lys166), located at the N-terminus of α6, a region of conformational flexibility, are required for PP2Ac−Tap42/α4 interactions, whereas CR3 and CR4 are unnecessary. Our results are consistent with a previous deletion mutagenesis study demonstrating that residues 94−202 of murine α4 are sufficient to mediate PP2Ac interactions (*19*). The position of CR2 on the convex face of Tap42ΔC contrasts with TPR and 14-3-3-like proteins that interact with their partner proteins via concave surfaces and/or interhelix loops (*31*, *33*, *35*).

PP2Ac interacts with Tap42/α4 mutually exclusively with PR65/A (*9*), implying overlapping sites on PP2Ac for recognition of PR65/A and Tap42/α4. Insights into regions of PP2Ac responsible for Tap42/α4 interactions have been provided by mutagenesis and domain mapping experiments. Yeast two-hybrid screens identified the N-terminal α-helical domain (residues 19−165) of PP2Ac as being sufficient for interactions with α4 (*10*), whereas domain mapping experiments defined a short region of Sit4 and Pph21 (equivalent to residues 24−56 of mammalian PP2Ac) as being critical for Tap42 interactions (*14*). Mutation of an invariant glutamate (Glu42) in yeast Pph21, mammalian PP2Ac, and the related phosphatase Sit4 abolished α4−Tap42 interactions (*10*, *14*). Disruption of α4 binding to PP2Ac correlated with increased PR65/A association (*10*). Furthermore, mutation of three basic residues in PP2Ac (Lys41, Arg49, Lys74) progressively weakened interactions with PR65/A while enhancing α4 interactions (*10*). These data suggest that

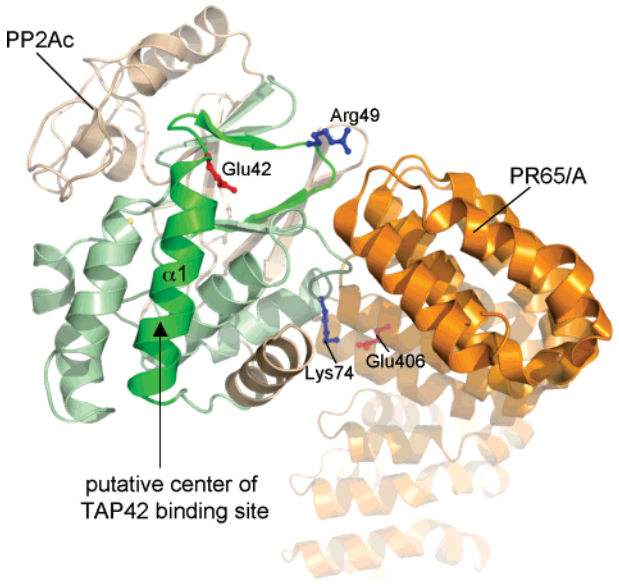

FIGURE 7: Structure of the PP2Ac-PR65/A subunit heterodimer (PDB ID 2IE3) (*40*). In PP2Ac regions shown to interact with Tap42/α4 are highlighted: light green (residues 19−165) (*10*) and bright green (residues 24−56) (*14*) (see text for details). Mutation of Glu42 reduces Tap42/α4 interactions, whereas mutation of Arg49 and Lys74 blocks PR65/A interactions while enhancing association with Tap42/α4. Lys41, adjacent to Glu42, is omitted for clarity. These data suggest that a site centered close to Glu42 involving the α1 helix, proximal to the PR65/A interface, will mediate contacts to Tap42/α4.

distinct sets of residues within the N-terminal PP2Ac α-helical domain contribute to interactions with PR65/A and Tap42/α4, as expected from their different three-dimensional structures (*27*), and are consistent with the notion that a negatively charged surface of PP2Ac interacts with positively charged residues of Tap42/α4. The predominant interactions between PP2Ac and PR65/A involve the N-terminal α-helical subdomain of PP2Ac, but with additional contacts to more C-terminal regions (Figure 7) (*40*). Significantly, the region of Sit4 defined to be sufficient for Tap42 interactions (*14*) (equivalent to residues 24−56 of PP2Ac, including the α1 helix and Glu42) is situated immediately adjacent to the PR65/A binding site of PP2Ac (Figure 7). The interaction of Tap42/α4 with PP2Ac at a site centered on this region could account for the mutually exclusive binding of PR65/A and Tap42/α4 to PP2Ac, while explaining how different sets of residues of PP2Ac determine recognition of these distinct regulatory subunits and the ability of Tap42/α4, but not PR65/A, to recognize the related phosphatase catalytic subunits of PP2A, PP4, and PP6.

Overall, PP2Ac features a uniform negative electrostatic potential, whereas PR65/A is also mainly negatively charged, except HEAT repeats 11−15, responsible for interacting with PP2Ac. Our observation that charge reversal of Arg163 and Lys166 on Tap42/α4 eliminates PP2Ac interactions indicates that contacts with acidic residues on PP2Ac are likely to dominate interactions with Tap42/α4.

Both Tap42/α4 and PR65/A fulfill similar functions as scaffolding proteins for PP2Ac, modifying its substrate specificity and cellular localization while adopting different α-helical topologies. Tap42/α4 interacts with PP2Ac via its N-terminal ordered helical domain and binds PP2A substrates via its C-terminal 120 residues, thereby colocalizing PP2Ac with defined phosphorylated substrates. The interaction of the p38 MAPK kinase, MEK3, with the C-terminal region of α4 promotes PP2Ac-mediated site-specific dephosphorylation of MEK3 (*41*). Our data, in agreement with others (*26*), suggest that the C-terminal region of Tap42/α4 lacks stable secondary structure, adopting an extended flexible structure. However, the striking structural conservation of this region (Figure 1) would suggest that distinct structural conformations are likely to be assumed on engaging an interacting phosphoprotein substrate. In contrast to Tap42/α4, within the context of the PP2A heterotrimer, PR65/A functions to colocalize the catalytic and regulatory B subunits rather than bind substrate directly.

ACKNOWLEDGMENT

We thank Martin Walsh at BM14, ESRF, for help with data collection.

REFERENCES

1. Janssens, V., Goris, J., and Van Hoof, C. (2005) PP2A: the expected tumor suppressor, *Curr. Opin. Genet. Dev. 15*, 34−41.
2. Mumby, M. (2007) The 3D structure of protein phosphatase 2A: new insights into a ubiquitous regulator of cell signaling, *ACS Chem. Biol. 2*, 99−103.
3. Kamibayashi, C., Estes, R., Lickteig, R. L., Yang, S. I., Craft, C., and Mumby, M. C. (1994) Comparison of heterotrimeric protein phosphatase 2A containing different B subunits, *J. Biol. Chem. 269*, 20139−20148.
4. Zhao, Y., Boguslawski, G., Zitomer, R. S., and DePaoli-Roach, A. A. (1997) *Saccharomyces cerevisiae* homologs of mammalian B and B′ subunits of protein phosphatase 2A direct the enzyme to distinct cellular functions, *J. Biol. Chem. 272*, 8256−8262.
5. Turowski, P., Myles, T., Hemmings, B. A., Fernandez, A., and Lamb, N. J. (1999) Vimentin dephosphorylation by protein phosphatase 2A is modulated by the targeting subunit B55, *Mol. Biol. Cell 10*, 1997−2015.
6. Seeling, J. M., Miller, J. R., Gil, R., Moon, R. T., White, R., and Virshup, D. M. (1999) Regulation of beta-catenin signaling by the B56 subunit of protein phosphatase 2A, *Science 283*, 2089−2091.
7. Ory, S., Zhou, M., Conrads, T. P., Veenstra, T. D., and Morrison, D. K (2003) Protein phosphatase 2A positively regulates Ras signaling by dephosphorylating KSR1 and Raf-1 on critical 14−3−3. binding sites, *Curr. Biol. 13*, 1356−1364.
8. Di Como, C. J., and Arndt, K. T. (1996) Nutrients, via the Tor proteins, stimulate the association of Tap42 with type 2A phosphatases, *Genes Dev. 10*, 1904−1916.
9. Murata, K., Wu, J., and Brautigan, D. L. (1997) B cell receptor-associated protein alpha4 displays rapamycin-sensitive binding directly to the catalytic subunit of protein phosphatase 2A, *Proc. Natl. Acad. Sci. U.S.A. 94*, 10624−10629.
10. Prickett, T. D., and Brautigan, D. L. (2004) Overlapping binding sites in protein phosphatase 2A for association with regulatory A and alpha-4 (mTap42) subunits, *J. Biol. Chem. 279*, 38912−38920.
11. Jiang, Y., and Broach, J. R. (1999) Tor proteins and protein phosphatase 2A reciprocally regulate Tap42 in controlling cell growth in yeast, *EMBO J. 18*, 2782−2792.
12. Chen, J., Peterson, R. T., and Schreiber, S. L. (1998) Alpha 4 associates with protein phosphatases 2A, 4, and 6, *Biochem. Biophys. Res. Commun. 247*, 827−832.
13. Duvel, K., Santhanam, A., Garrett, S., Schneper, L., and Broach, J. R. (2003) Multiple roles of Tap42 in mediating rapamycin-induced transcriptional changes in yeast, *Mol. Cell 11*, 1467−1478.
14. Wang, H., Wang, X., and Jiang, Y. (2003) Interaction with Tap42 is required for the essential function of Sit4 and type 2A phosphatases, *Mol. Biol. Cell 14*, 4342−4351.
15. Kong, M., Fox, C. J., Mu, J., Solt, L., Xu, A., Cinalli, R. M., Birnbaum, M. J., Lindsten, T., and Thompson, C. B. (2004) The PP2A-associated protein alpha4 is an essential inhibitor of apoptosis, *Science 306*, 695−698.

16. Wang, H., and Jiang, Y. (2003) The Tap42-protein phosphatase type 2A catalytic subunit complex is required for cell cycle-dependent distribution of actin in yeast, *Mol. Cell. Biol. 23*, 3116−3125.
17. Prickett, T. D., and Brautigan, D. L. (2006) The alpha4 regulatory subunit exerts opposing allosteric effects on protein phosphatases PP6 and PP2A, *J. Biol. Chem. 281*, 30503−30511.
18. Yan, G., Shen, X., and Jiang, Y. (2006) Rapamycin activates Tap42-associated phosphatases by abrogating their association with Tor complex 1, *EMBO J. 25*, 3546−3555.
19. Inui, S., Sanjo, H., Maeda, K., Yamamoto, H., Miyamoto, E., and Sakaguchi, N. (1998) Ig receptor binding protein 1 (alpha4) is associated with a rapamycin-sensitive signal transduction in lymphocytes through direct binding to the catalytic subunit of protein phosphatase 2A, *Blood 92*, 539−546.
20. Liu, J., Prickett, T. D., Elliott, E., Meroni, G., and Brautigan, D. L. (2001) Phosphorylation and microtubule association of the Opitz syndrome protein mid-1 is regulated by protein phosphatase 2A via binding to the regulatory subunit alpha 4, *Proc. Natl. Acad. Sci. U.S.A. 98*, 6650−6655.
21. Collaborative Computational Project, Number 4 (1994) The CCP4 suite: programs for protein crystallography, *Acta Crystallogr. D50*, 760−763.
22. Perrakis, A., Morris, R., and Lamzin, V. S. (1999) Automated protein model building combined with iterative structure refinement, *Nat. Struct. Biol. 6*, 458−463.
23. Emsley, P., and Cowtan, K. (2004) COOT: Model-building tools for molecular graphics, *Acta Crystallogr. D60*, 2126−2132.
24. Yang, Z. R., Thomson, R., McNeil, P., and Esnouf, R. M. (2005) RONN: the bio-basis function neural network technique applied to the detection of natively disordered regions in proteins, *Bioinformatics 21*, 3369−3376.
25. Kelley, L. A., MacCallum, R. M., and Sternberg, M. J. (2000) Enhanced genome annotation using structural profiles in the program 3D-PSSM, *J. Mol. Biol. 299*, 499−520.
26. Smetana, J. H., Oliveira, C. L., Jablonka, W., Aguiar Pertinhez, T., Carneiro, F. R., Montero-Lomeli, M., Torriani, I., and Zanchin, N. I. (2006) Low resolution structure of the human alpha4 protein (IgBP1) and studies on the stability of alpha4 and of its yeast ortholog Tap42, *Biochim. Biophys. Acta 1764*, 724−734.
27. Groves, M. R., Hanlon, N., Turowski, P., Hemmings, B. A., and Barford, D. (1999) The structure of the protein phosphatase 2A PR65/A subunit reveals the conformation of its 15 tandemly repeated HEAT motifs, *Cell 96*, 99−110.
28. Holm, L., and Sander, C. (1993) Protein structure comparison by alignment of distance matrices, *J. Mol. Biol. 233*, 123−138.
29. Rice, L. M., and Brunger, A. T. (1999) Crystal structure of the vesicular transport protein Sec17: implications for SNAP function in SNARE complex disassembly, *Mol. Cell 4*, 85−95.
30. Fukuhara, N., Ebert, J., Unterholzner, L., Lindner, D., Izaurralde, E., and Conti, E. (2005) SMG7 is a 14-3-3-like adaptor in the nonsense-mediated mRNA decay pathway, *Mol. Cell 17*, 537−547.
31. Lapouge, K., Smith, S. J., Walker, P. A., Gamblin, S. J., Smerdon, S. J., and Rittinger, K. (2000) Structure of the TPR domain of $p67^{phox}$ in complex with Rac·GTP, *Mol. Cell 6*, 899−907.
32. Das, A. K., Cohen, P. W., and Barford, D. (1998) The structure of the tetratricopeptide repeats of protein phosphatase 5: implications for TPR-mediated protein-protein interactions, *EMBO J. 17*, 1192−1199.
33. Scheufler, C., Brinker, A., Bourenkov, G., Pegoraro, S., Moroder, L., Bartunik, H., Hartl, F. U., and Moarefi, I. (2000) Structure of TPR domain-peptide complexes: critical elements in the assembly of the Hsp70-Hsp90 multichaperone machine, *Cell 101*, 199−210.
34. Yang, J., Roe, S. M., Cliff, M. J., Williams, M. A., Ladbury, J. E., Cohen, P. T., and Barford, D. (2005) Molecular basis for TPR domain-mediated regulation of protein phosphatase 5, *EMBO J. 24*, 1−10.
35. Yaffe, M. B., Rittinger, K., Volinia, S., Caron, P. R., Aitken, A., Leffers, H., Gamblin, S. J., Smerdon, S. J, and Cantley, L. C. (1997) The structural basis for 14-3-3:phosphopeptide binding specificity, *Cell 91*, 961−971.
36. Liu, D., Bienkowska, J., Petosa, C., Collier, R. J., Fu, H., and Liddington, R. (1995) Crystal structure of the zeta isoform of the 14-3-3 protein, *Nature 376*, 191−194.
37. Xiao, B., Smerdon, S. J., Jones, D. H., Dodson, G. G., Soneji, Y., Aitken, A., and Gamblin, S. J. (1995) Structure of a 14-3-3 protein and implications for coordination of multiple signalling pathways, *Nature 376*, 188−191.
38. Zhang, M., Windheim, M., Roe, S. M., Peggie, M., Cohen, P., Prodromou, C., and Pearl, L. H. (2005) Chaperoned ubiquitylation—Crystal structures of the CHIP U box E3 ubiquitin ligase and a CHIP-Ubc13-Uev1a complex, *Mol. Cell 20*, 525−538.
39. Groves, M. R., and Barford, D. (1999) Topological characteristics of helical repeat proteins, *Curr. Opin. Struct. Biol. 9*, 383−389.
40. Xing, Y., Xu, Y., Chen, Y., Jeffrey, P. D., Chao, Y., Lin, Z., Li, Z., Strack, S., Stock, J. B., and Shi, Y. (2006) Structure of protein phosphatase 2A core enzyme bound to tumor-inducing toxins, *Cell 127*, 341−353.
41. Prickett, T. D., and Brautigan, D. L. (2007) Cytokine activation of p38 MAPK and apoptosis is opposed by alpha-4 targeting of PP2A for site-specific dephosphorylation of MEK3, *Mol. Cell. Biol. 27*, 4217−4227 (PMID 17438131).
42. Barton, G. J. (1993) ALSCRIPT: a tool to format multiple sequence alignments, *Protein Eng. 6*, 37−40.
43. Nicholls, A., Sharp, K., and Honig, B. (1991) Protein folding and association: insights from the interfacial and thermodynamic properties of hydrocarbons, *Proteins 11*, 281−296.

BI7007118